Journal of Materials Chemistry C

Hole Injection Monolayer Enables Cost-effective Perovskite Light-Emitting Diodes

Journal:	*Journal of Materials Chemistry C*
Manuscript ID	TC-ART-12-2022-005491.R1
Article Type:	Paper
Date Submitted by the Author:	19-Jan-2023
Complete List of Authors:	Zhang, Congyang; Okinawa Institute of Science and Technology Graduate University, Energy Materials and Surface Sciences Unit Mariotti, Silvia ; Okinawa Institute of Science and Technology Graduate University, Energy Materials and Surface Sciences Unit Ono, Luis; Okinawa Institute of Science and Technology Graduate University, Energy Materials and Surface Sciences Unit Ding, Chenfeng; Okinawa Institute of Science and Technology Graduate University, Energy Materials and Surface Sciences Unit Mitrofanov, Kirill ; Okinawa Institute of Science and Technology Graduate University, Organic Optoelectronics Unit Zhang, Caiyi; Okinawa Institute of Science and Technology Graduate University, Energy Materials and Surface Sciences Unit Yuan, Shuai; Okinawa Institute of Science and Technology Graduate University, Energy Materials and Surface Sciences Unit Ji, Penghui; Okinawa Institute of Science and Technology Graduate University, Energy Materials and Surface Sciences Unit Zhang , Jiahao ; Okinawa Institute of Science and Technology Graduate University, Energy Materials and Surface Sciences Unit Wu, Tianhao; Okinawa Institute of Science and Technology Graduate University, Energy Materials and Surface Sciences Unit Kabe, Ryota; Okinawa Institute of Science and Technology Graduate University, Organic Optoelectronics Unit Qi, Yabing; Okinawa Institute of Science and Technology Graduate University, Energy Materials and Surface Sciences Unit

ARTICLE

Hole Injection Monolayer Enables Cost-effective Perovskite Light-Emitting Diodes

Received 00th January 20xx,
Accepted 00th January 20xx

DOI: 10.1039/x0xx00000x

Congyang Zhang,[a] Silvia Mariotti,[a] Luis K. Ono,[a] Chenfeng Ding,[a] Kirill Mitrofanov,[b] Caiyi Zhang,[a] Shuai Yuan,[a] Penghui Ji,[a] Jiahao Zhang,[a] Tianhao Wu,[a] Ryota Kabe,[b] and Yabing Qi[a*]

Developing cost-effective fabrication is one of the key steps for metal halide perovskite light emitting diodes (PeLEDs) toward their future commercialization and industrial applications. Considering the low material consumption, upscalable processing and energy level offset tunability of surface anchored monolayer, we proposed a [2-(9H-carbazol-9-yl)ethyl]phosphonic acid, 2PACz based hole injection monolayer (HIML) for the cost-effective fabrication of efficient PeLEDs. On the basis of the systematic surface science study and characterization, we elucidate the effect of 2PACz molecular layer on the work function engineering of ITO, energetic alignment and hole injection between ITO and perovskite emission layer, and radiative recombination of the perovskite layer at the bottom interface. In particular, our thickness dependent UPS measurement results suggest that the molecular dipole of 2PACz is the main contributor for the work function change of ITO. Finally, by demonstrating the efficient LEDs with blue emission and enlarged device area, we verified the universality of the HIML based strategy. This study highlights the great potential of the HIML for cost-effective PeLEDs, which can help translate perovskite light emission technologies toward the commercial level in the future.

1. Introduction

Known for their excellent luminescence efficiency, tunable emission color, and narrow emission linewidth, metal halide perovskite materials have received wide-ranging research interest during the past several years[1-3]. Since the first perovskite light emitting diode (PeLED) was demonstrated by Tan and coworkers in 2014[4], great progress has been made toward high device performance. These improvements benefited from various perovskite emission layer related strategies, such as composition engineering[5], dimension control[6-10], heterostructure designing[11-16], defect passivation[17-21], *etc*. To date, the green, red, and near infrared PeLEDs with record high external quantum efficiencies (EQEs) of over 20% have been demonstrated[8, 11, 16, 18, 20-24], which are comparable with the mature organic light emitting diode (OLED) and quantum dot light emitting diode (QLED) technologies. Despite these remarkable achievements based on perovskite material related strategies, the cost-effective device fabrication and production are often overlooked, and will be one of the vital aspects for commercialization of PeLEDs in the future[25].

In general, one of the major superiorities of PeLEDs is low cost of metal halide perovskite emission materials. However, considering the total cost of PeLEDs, the commonly used organic hole injection/transport layers (HILs/HTLs) account for a large proportion (see details in Fig. S1-2 and Table S1) of the whole material cost. In addition, because of the direct contact of HILs/HTLs with the perovskite emission layer (EML) in the standard device architectures, HILs/HTLs play a significant role on the hole injection, perovskite nucleation and growth, and luminescence quenching and interface passivation[26-28]. Hence, it is imperative to develop low cost HIL for efficient PeLEDs for reducing the so-called performance-cost gap. For efficient hole injection and transport, some conjugated polymers, such as poly[bis(4-phenyl)(2,4,6-trimethylphenyl)amine] (PTAA), poly(9,9-dioctylfluorene-alt-N-(4-*sec*-butylphenyl)diphenylamine) (TFB), poly(N-(4-butylphenyl)diphenyl-amine) (poly-TPD), have been widely used. Nevertheless, most of them are expensive (Table S2 and Fig. S2b). Furthermore, as the underlying interfaces, their strong hydrophobicity would greatly suppress the nucleation and crystallization process of perovskite layers. To achieve a high quality perovskite layer using solution processing, interfacial modification needs to be designed elaborately, which makes the fabrication process of PeLEDs complicated[26]. A comprehensive comparison between the commonly used HIL/HTL is shown in Fig. 1a, regarding the wettability, suppression of fluorescence quenching of perovskite emission layer, and fabrication method compatibility with large scale. To date, poly(3,4-ethylenedioxy thiophene):poly(styrene sulfonic acid) (PEDOT:PSS) is the most widely used and affordable HIL for facilitating hole injection. However, because of the well-known

[a] *Energy Materials and Surface Sciences Unit (EMSSU), Okinawa Institute of Science and Technology Graduate University (OIST), 1919-1 Tancha, Onna-son, Kunigami-gun, Okinawa 904-0495, Japan.*
[b] *Organic Optoelectronics Unit, Okinawa Institute of Science and Technology Graduate University, 1919-1 Tancha, Onna-son, Kunigami-gun, Okinawa 904-0495, Japan.*
**Corresponding author: Yabing Qi, E-Mail: Yabing.Qi@OIST.jp*
Electronic Supplementary Information (ESI) available: [details of any supplementary information available should be included here]. See DOI: 10.1039/x0xx00000x

hygroscopic and acidic properties, indium tin oxide (ITO) electrodes can be easily corroded by PEDOT:PSS [27]. Besides, charge carrier quenching at the PEDOT:PSS/perovskite interface is a severe issue, and limits the device performance and operation lifetime[29]. Metal oxides, such as nickel oxide (NiO_x), show a great potential as well. But it requires a high annealing temperature (over 400 ℃), making the fabrication cost much higher, and also incompatible with the large scale PeLED device production[30, 31].

Surface anchored or self-assembled monolayers are small molecules with anchoring groups that can be chemically attached on metal oxide or metal surface as stable molecule-thick layers[32]. they possess the advantages such as very low material consumption, upscale processing and green-solvent processability[33]. As surface modification layers, they are able to modulate and stabilize the work function of the anchored surface through forming dipole moments, thus promoting a better energy alignment at the interface[34]. Importantly, the rich diversity in anchoring groups and surface chemistry endows them with high designability and functionality. Therefore, these monolayers have been extensively studied in various optoelectronic application fields, including photovoltaics[35], LEDs[36-38], and transistors[39, 40]. Recently, they have also been employed in perovskite solar cells (PSCs) as charge-selective contacts, which were initiated by Magomedov and Yalcin in 2018[41, 42]. Furthermore, through optimization of the monolayers molecule and device fabrication process, the high power conversion efficiency (PCE) of over 23% and 29% have been demonstrated for single junction and tandem-devices, respectively[43-47]. These monolayers used in PSCs also play a significant role of interface passivation that greatly suppresses non-radiative recombination of perovskite layers[48]. Therefore, they are expected to be a suitable HIL to meet the requirements for efficient and cost-effective PeLEDs as well. It is interesting to note that during the preparation of this manuscript, two newly published studies demonstrated their PeLED devices using a monolayers based HIL and verified the feasibility of this strategy from the device application point of view[49, 50]. Rapid progress on perovskite optoelectronic devices with monolayer based HTL/HIL calls for a comprehensive understanding of the effect of monolayers on the interface engineering, hole injection and device performance.

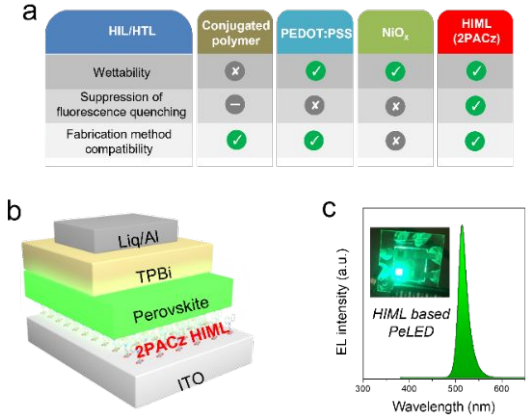

Figure 1 Proof-of-concept HIML based PeLEDs. **a** The comparison of commonly used HIL/HTL and carbazole based HIML used in PeLEDs regarding the wettability, suppression of fluorescence quenching of perovskite layers, and fabrication method compatibility. **b** Device structure of the HIML based PeLED. **c** Electroluminescence spectrum of the HIML based PeLED. The inset photograph is the HIML based PeLED under operation, showing uniform and bright green emission.

Herein, we demonstrate a proof-of-concept cost-effective PeLED with a [2-(9H-carbazol-9-yl)ethyl]phosphonic acid, 2PACz based HIML that is directly anchored on ITO electrode (Fig. 1b). We chose 2PACz as the monolayer molecule because of the good wettability and suitable energy levels of the modified ITO that can be achieved simultaneously for the formation of uniform perovskite emission layer and hole injection in perovskite LEDs. Based on the HIML strategy, bright green emission PeLED (Fig. 1c) with a much higher efficiency and longer operation lifetime was achieved compared to both the bare ITO and commonly used ITO/PEDOT:PSS based devices. A systematic surface science study and characterization enable us to elucidate the critical role of 2PACz molecular layer on the work function (WF) engineering of ITO, energetic alignment and hole injection between ITO and perovskite emission layer, and radiative recombination of the perovskite layer at the bottom interface. Finally, we also demonstrate the applicability of the HIML based strategy in blue and large area PeLEDs with improved efficiency.

2. Experimental Section

2.1 Materials

Cesium bromide (CsBr, 99.999%), Lead bromide ($PbBr_2$, 99.999%), Lead chloride ($PbCl_2$, 99.999%), 18-Crown-6 (Crown), Phenethylammonium bromide (PEABr), and Rubidium Bromide (RbBr, 99.6%) were purchased from Sigma-Aldrich. [2-(9H -Carbazol-9-yl)ethyl]phosphonic acid (2PACz), 1,6-Diaminohexane (DAHE), Formamidine Hydrobromide (FABr), and N,N-dimethyl-1,3-propanediaminedihydrobromide ($DPDABr_2$) were purchased from Tokyo Chemical Industry. Dimethyl sulfoxide (DMSO, Super Dehydrated), Ethanol and Chlorobenzene were purchased from Wako. PEDOT:PSS (Clevios PVP AI 4083) was purchased from Heraeus. TPBi and Liq were obtained from Luminescence Technology. All the chemicals were used without further purification.

2.2 Device fabrication

The patterned ITO glass substrates were cleaned by sequential ultrasonication within detergent aqueous solution, deionized water, acetone, and ethanol for 30 min each, and were dried under nitrogen flow. Pre-cleaned ITO substrates were treated with ultraviolet-ozone for 60 min. For HIML based devices, the 2PACz was deposited on ITO glass substrates by spin-coating a 2PACz/ethanol solution (3 mM) at 8000 rpm for 30s. Then, it was annealed on a hot plate at 150 ℃ for 20 min. For PEDOT:PSS based devices, PEDOT:PSS (Clevios PVP AI 4083) was spin-coated onto the cleaned ITO-coated glass at 4000 rpm for 30 s and annealed at 150 ℃ for 20 min. Then, these substrates were transferred into a glovebox for the perovskite emission

layer deposition. For green emitting devices, the perovskite precursor was prepared by mixing CsBr (0.2 mmol), $PbBr_2$ (0.2 mmol), and PEABr (0.08 mmol), and crown (4 mg) in DMSO (1 mL). After complete dissolving, the precursor was spin-coated at 1000 rpm for 5 s and 5000 rpm for 115 s, and then annealed at 80 ℃ for 10 min. For sky blue emitting devices, the perovskite precursor was prepared by mixing CsBr (0.18 mmol), RbBr (0.015 mmol), FABr (0.03 mmol) $PbBr_2$ (0.09 mmol), $PbCl_2$ (0.06 mmol) and DAHE (0.015 mmol) in DMSO (1 mL). After complete dissolving, the precursor was spin-coated at 1000 rpm for 5 s and 4000 rpm for 115 s, and then annealed at 80 ℃ for 10 min. For pure blue emitting devices, the perovskite precursor was prepared by mixing CsBr (0.154 mmol), RbBr (0.066 mmol), $PbBr_2$ (0.05 mmol), $PbCl_2$ (0.15 mmol), $DPDABr_2$ (0.04 mmol), and crown (4 mg) in DMSO (1 mL). After completely dissolving, the precursor was spin-coated at 1000 rpm for 5 s and 4000 rpm for 115 s, and then annealed at 100 ℃ for 10 min. Finally, TPBi (40 nm), Liq (2 nm), and Al (100 nm) were deposited by thermal evaporation. The active area of devices is 0.04 cm^2. The hole-only devices adopt the configuration of ITO/2PACz/Perovskite/HATCN/Al. The fabrication of 2PACz and perovskite layers was similar to the PeLEDs. The HATCN layer (8 nm) in hole-only devices was deposited through thermal evaporation under high vacuum.

2.3 Characterization and device measurement

The XRD characterization was conducted by a Bruker AXS D8 Discover diffractometer. UV-vis spectra were recorded by a JASCO V-670 spectrophotometer. Steady-state PL spectra and PLQYs were taken by an JASCO FP -8500 spectrophotometer. Time-resolved PL spectra were measured by a time-resolved spectrometer (Hamamatsu, Streakscope) equipped with a femtosecond mode-locked Ti:sapphire laser, excited at 400 nm and measured at room temperature. The chemical compositions and energy levels were determined by the XPS and UPS on a photoelectron spectrometer (XPS-AXIS Ultra HAS, Kratos) equipped with monochromatic Al-Kα = 1486.6 eV and nonmonochromatic He-I = 21.22 eV sources. The binding energy scales for UPS and XPS were calibrated by measuring the Fermi edge (E_F = 0 eV) and Au $4f_{7/2}$ (84.0 eV) on a clean Au surface. For the thickness-dependent UPS measurement, 2PACz was evaporated on ITO surface in a vacuum chamber with a base pressure of ~1×10^{-4} Pa. Before the evaporation experiment, the quartz crystal microbalance (QCM) was calibrated by comparing the thickness displayed at the QCM with the real thickness measured by AFM (with a film scratching method). After the calibration, we further confirmed that the nominal thickness is almost consistent with the real thickness measured by AFM (Fig. S22). SEM images were obtained by a scanning electron microscope (Helios NanoLab G3 UC, FEI). Contact angle measurements were conducted by a drop shape analyzer (FM 4000, Krüss GmbH, Germany). Tapping mode AFM images were acquired using an ASYLUM-MFP-3D equipment with standard silicon cantilevers and a nominal spring constant of 48 N/m and resonant frequency of 190 kHz (AFM cantilever model number and manufacturer: Tap 190Al-G from Budget Sensors). The luminance-current-voltage (L-I-V) characteristics and EL spectra were measured simultaneously with a Keithley 2400 source meter and Konica Minolta CS-2000 spectroradiometer. All the devices were encapsulated with cover glasses by UV glue (Norland NOA81), and measured in air at room temperature. The EQE values were calculated based on the spectroradiometer method according to our previous works[51, 52]. Transient absorption experiments were conducted using a pump-probe method using the experimental setup with the CMOS detector (S12198-1024Q, Hamamatsu) and InGaAs photodiode array (G9203-256DA, Hamamatsu). Short laser pulses were generated by the Yb:KGW laser (Light conversion, Pharos, 1030 nm, 1 kHz repetition rate, 150 fs, 2 mJ per pulse): 365 nm pump beam was generated with the use of the optical parametric amplifier (Light conversion, ORPHEUS), and the probe beam was focused into a YAG plate to generate white light continuum.

3. Results and Discussion

3.1 Device performance of the PeLED with 2PACz based HIML

2PACz was selected as the target HIML molecule. Its chemical structure is shown in Fig. S3, which contains a carbazole moiety, a hydrocarbon chain and a phosphonic acid anchoring group. It is well know that the phosphonic acid groups are able to be attached on a metal oxide surface through strong bidentate/tridentate bonds, forming a uniform and stable monolayer at room temperature[53]. Recently, 2PACz and its derivative molecules have been successfully demonstrated in high-performance p-i-n perovskite solar cells to modify the transparent conducting oxide (TCO) with a better aligned energy level for charge transfer[45, 46]. In addition, owing to the existence of electron-rich carbazole heterocycles, an excellent passivation effect at the TCO/perovskite interface has been verified as well[33].

In this work, based on the reported recipe[54], 2PACz was directly deposited on the ITO electrode with a 2PACz/ethanol solution (1 mg/mL, corresponding to ~3 mM). Based on the ITO substrate modified with 2PACz as HIML (ITO/2PACz), we fabricated the green-emitting PeLEDs with the device structure of ITO/2PACz/perovskite/2,2',2''-(1,3,5-benzinetriyl)-tris(1-phenyl-1-H-benzimidazole) (TPBi)/8-hydroxyquinolinolato-lithium (Liq)/Al (Fig. 1b). The cross-section SEM image of the HIML based PeLED is shown in Fig. 2a, from which individual layers can be clearly observed. Because of the monolayer feature, it is difficult to distinguish the 2PACz layer between ITO and perovskite. Under electric bias, the PeLED shows bright green-emission electroluminescence (EL) spectrum with a peak centered at 514 nm and a narrow full width at half maximum (FWHM) of 21 nm (Fig. 1c). In comparison, the bare ITO based PeLED was fabricated. Fig. 2b, c show the current density-voltage-luminance (J-V-L) and EQE-J curves, respectively. A much lower leakage current is observed for the ITO/2PACz based device than the one with bare ITO, which can be attributed to the much lower trap density at the interface between ITO and the perovskite emission layer. In addition, the ITO/2PACz based device has a lower turn-on voltage (~3 V) than

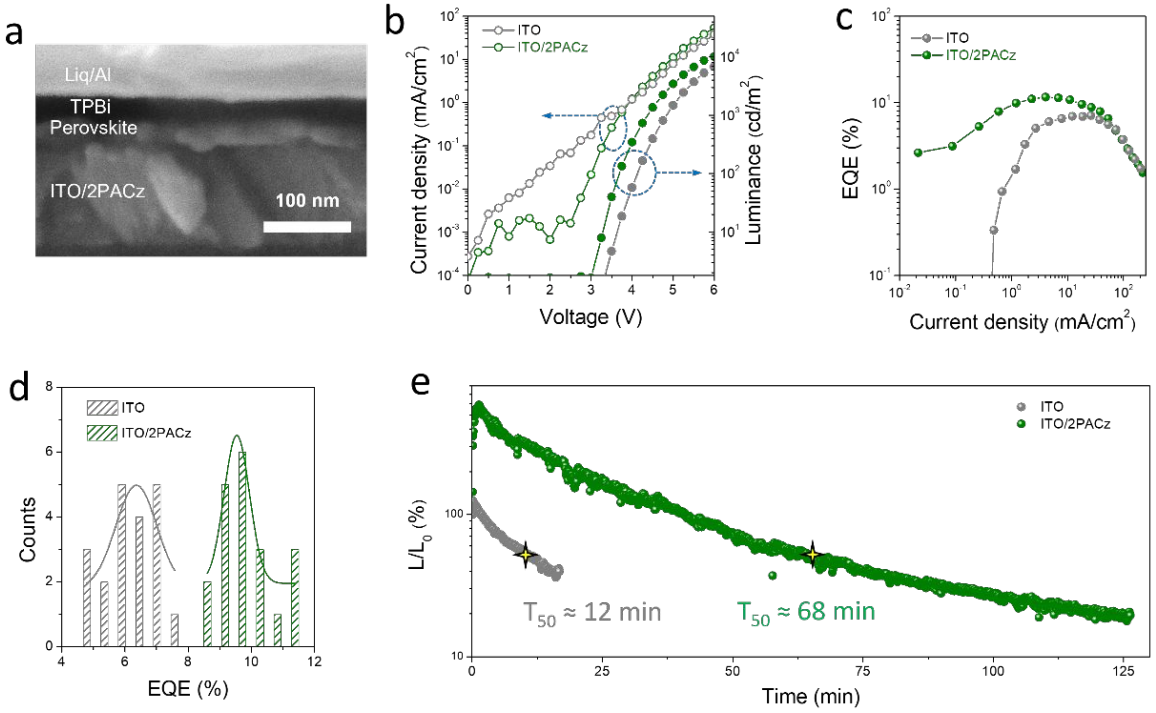

Figure 2 Device performance of the PeLED device based on 2PACz as HIML. **a** Cross-section SEM image of the HIML based PeLED. **b-e (b)** Current density and luminance versus driving voltage curves, **(c)** EQE-current density curves, **(d)** histogram of the maximum EQE, and **(e)** normalized luminance-time curves operated under constant current at the initial luminance of ~100 cd/m^2 of the PeLEDs with and without 2PACz as HIML.

the bare ITO based device (~3.4 V). After turning on, its current density becomes larger at the same given voltages. All these device results indicate the facilitated charge injection property of 2PACz on ITO. Based on these improvements, the ITO/2PACz based device reaches a peak EQE of 11.6% at a current density of ~4.1 mA/cm^2. In contrast, EQE of the bare ITO based device is only 7.1%. In addition, the ITO/PEDOT:PSS based PeLED was also fabricated, and showed even worse EL performance with a peak EQE of 1.8% (Fig. S4). Fig. 2d shows the histogram of the peak EQE values for 20 devices, revealing an average peak EQE of 6.4% and 9.5% for the ITO and ITO/2PACz based devices, respectively. Besides, compared to the bare ITO, the ITO/2PACz based devices show significantly lower relative standard deviation (11.6% *vs.* 36.3%), indicating the good reproducibility of our HIML based devices. The operational stability of PeLEDs is another key issue that limits their practical application. Therefore, we measured the operational lifetime of these two devices in ambient air at the initial luminance of 100 cd/m^2. As shown in Fig. 2e, luminance of the bare ITO based device reduces rapidly under constant current with a half time (T_{50}) of ~12 min. In contrast, the ITO/2PACz based device shows a remarkably increase of T_{50} value to ~68 min. Even though the ITO/2PACz based device showed longer operation lifetime, the luminance overshoot (*i.e.,* luminance first increased with time and then decreased) was observed. It can be mainly attributed to ion migration, especially related to halide ions that migrate towards and accumulate at grain boundaries and device interfaces. Charge injection from the electrodes tends to be facilitated because of the strong local electric field at the interfaces, and results in the initial luminance overshoot.[55, 56] The luminance overshoot issue of the bare ITO based device was less distinctive than the ITO/2APCz based device, and this is likely because the inferior ITO/perovskite interface leads to rapid degradation of device performance even before the overshoot issue can be observed. Overall, the significant improvements of the device performance clearly demonstrate the great potential of the 2PACz based HIML for PeLEDs.

3.2 Characterization of 2PACz as HIML on ITO

In general, phosphonic acid based monolayer can be formed on ITO surface with strong chemisorption (Fig. 3a). The obvious improvement of PeLEDs performance should be greatly related to the 2PACz based HIML formed on ITO. To identify the atomic species of 2PACz on the ITO surface, we conducted X-ray photoelectron spectroscopy (XPS) measurements. All the peak fittings and analyses were conducted using the CasaXPS software. Mixed Gaussian/Lorentzian line shape and Shirley background were used for the XPS curve fitting. During the fitting, we constrained the ratio of Lorentzian/Gaussian line shape as 30%. Fig. 3b shows the high-resolution XPS spectrum of C 1s for the ITO/2PACz sample, which can be fitted into 5 sub-peaks. In addition, the peak FWHM for all the peaks in the C 1s region was kept as the same. The peaks are in reasonable agreement with the previous works[43, 46, 47, 54], and can be divided into two categories, including three kinds of carbon (C_{I}, C_{II}, and C_{III}) from 2PACz (marked in Fig. 3a) and two kinds carbon from adventitious species (C_{IV} and C_{V}). The strongest peak (C_{I}) at 283.8 eV can be assigned to the C-C or C-H bonds of aromatic carbon. The two peaks (C_{II}, and C_{III}) at 284.6 eV and 285.9 eV arise from the two types of carbon connecting with

nitrogen and phosphorous atoms of the 2PACz, respectively. In addition,

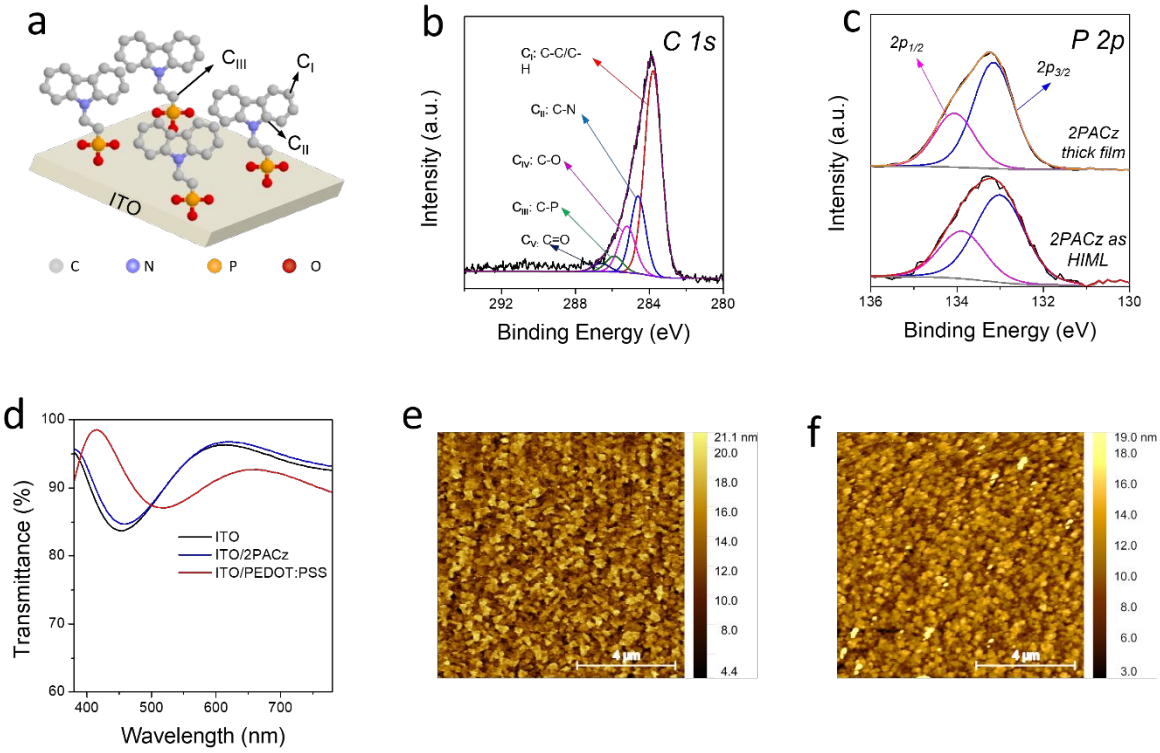

Figure 3 Characterization of 2PACz as HIML on ITO. **a** Schematic illustration of ITO/2PACz. Gray, yellow, blue, and red spheres represent C, P, N, and O atoms, respectively. **b** High-resolution XPS spectrum of the C 1s region of ITO/2PACz. **c** High-resolution XPS spectra of the P 2p region of ITO coated with 2PACz as HIML and thick film. **d** Optical transmittance of the ITO, ITO/2PACz, and ITO/PEDOT:PSS substrates. **e-f** Tapping mode AFM images of (e) ITO and (f) ITO/2PACz.

the residual two peaks (C_{IV} and C_V at 285.2 eV and 286.6 eV, respectively) are attributed to the carbon connecting with oxygen atoms via a C-O single bond and a C=O double bond originated from adventitious hydrocarbon[33, 57, 58]. In contrast, the bare ITO substrate does not show signals of 2PACz, instead, only has three typical hydrocarbon peaks of C-C/C-H, C-O, and C=O with reasonable FWHM (Fig. S5). Furthermore, the thickness of 2PACz on the ITO surface was estimated to be 1.1 nm (approximately 1 molecular layer thick) using the XPS intensity attenuation method based on Lambert-Beer Law (See details in Fig. S6) [59-61]. In particular, to reveal the possible chemical interaction at the very interface between ITO and 2PACz, a thick 2PACz film was prepared on ITO as well for comparison (by using a 2PACz/ethanol solution (10 mg/mL)). As shown in Fig. S7a, by comparing its element ratio of P/In with that of the thermal vacuum evaporated ITO/2PACz sample of which the thickness can be precisely controlled, we can roughly estimate that the thickness of the 2PACz thick layer is over 40 nm. Compared to the monolayer sample, both the C 1s and N 1s XPS spectra of the thick 2PACz film shift to lower binding energies, which can be attribute to the band bending at the 2PACz side when contact with ITO (Fig. S7b-c). However, the P 2p peaks (both the P $2p_{1/2}$ and P $2p_{3/2}$) show slight shift toward higher binding energies (Fig. 3c), which is highly consistent with previous reports and provides us strong evidence of the deprotonation process of the phosphate acid of 2PACz upon reaction with the oxygen of ITO according to a tridentate binding or a bidentate and tridentate mixed binding mechanism[53, 62, 63].

The optical transmission property of the ITO and ITO/2PACz substrate was investigated as well. As shown in Fig. 3d, transmittance across the whole visible range of the ITO substrate remains nearly the same after the 2PACz deposition, which is even much better than ITO/PEDOT:PSS substrate in the range from 500 nm to 750 nm. However, in the range of 400-500 nm, ITO/PEDOT:PSS has a better transmittance than the ITO and also ITO/2PACz. This phenomenon can be attributed to the relatively smaller refractive index (~1.33) of PEDOT:PSS than ITO (~1.97) and also the much lower absorption of PEDOT:PSS thin film in the wavelength range (400-500 nm), which synergistically reduce the overall reflective loss at the air/PEDOT:PSS and PEDOT:PSS/ITO interface and thus higher transmittance[64]. Overall, these results indicate the suitability of the ITO/2PACz to achieve the high light extraction efficiency for PeLEDs.

The surface topography of the ITO and ITO/2PACz substrates was studied by atomic force microscopy (AFM). The AFM images in Fig. 3e, f show insignificant difference for the surface topography between these two samples. These two substrates have similar root-mean-square (RMS) surface roughness (2.72 nm for ITO/2PACz, and 2.86 nm for the ITO substrate). The surface wettability is another important factor affecting the quality of polycrystalline perovskite film and

device performance, and we investigated it by measuring the contact angle using the perovskite precursor solvent (DMSO).

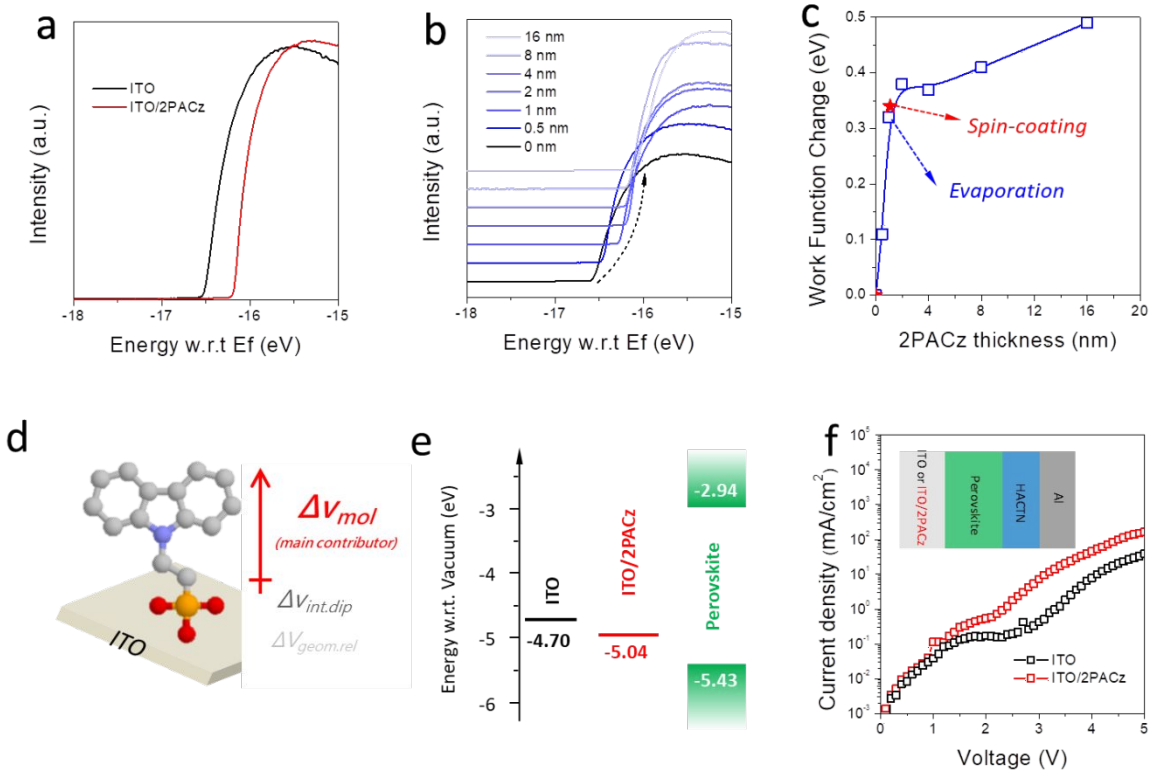

Figure 4 Energetic characterization and enhanced hole injection of the HIML based PeLEDs. **a** Electron cut-off region of the UPS spectra of the bare ITO substrate and solution processed 2PACz HIML on ITO. **b** Electron cut-off region of the UPS spectra of the evaporated 2PACz films on ITO with different thickness. **c** Plot of WF change of 2PACz on ITO as a function of 2PACz thickness. **d** Schematic illustration of the ITO/2PACz and the three contributors that result in the WF change. **e** Energy alignment scheme for the HIML based PeLED assuming the vacuum level alignment. **f** Dark current-voltage curves of the ITO and ITO/2PACz HIML based hole-only devices.

As shown in Fig. S8, the contact angle of DMSO does not show significant change for the ITO and ITO/2PACz surface (12.5° for ITO and 14.9° for ITO/2PACz). Overall, both the ITO and ITO/2PACz substrate surfaces have a good wettability that is beneficial for the nucleation and growth of a perovskite emission layer.

3.3 Effect of the HIML on energetic alignment

For efficient PeLEDs, efficient hole injection requires the suitable energetic alignment between ITO and the perovskite emission layer. In particular, the detail investigation of electronic structure and energy level alignment of the ITO/2PACz interface is highly desired. To determine such an alignment, we performed ultraviolet photoemission spectroscopy (UPS) measurements. Fig. 4a shows the cutoff region of UPS spectra of ITO and ITO/2PACz, from which we can identify that the WF of ITO surface significantly increase from 4.70 eV to 5.04 eV after 2PACz modification as a HIML. This WF change is consistent with the previous report[54], which is due to the contribution of the dipole moment formed with anchored 2PACz molecules.

To further investigate the WF change mechanism of 2PACz as HIML on ITO, we deposited the film using the vacuum thermal evaporation method, which allows precise control of the 2PACz film thickness. In this work, we prepared the ITO/2PACz samples with the 2PACz film thickness ranging from 0 nm to 16 nm. Before the UPS measurements, we first characterized the morphology of the ITO/2PACz substrates. As shown in Fig. S9, with the deposition of 2PACz on ITO in sequence, the surface became more uniform and smoother gradually. Fig. 3b shows the cutoff region of the UPS spectra, and the gradual increase of the WF of ITO surface as 2PACz deposition was observed.

In general, the work function change ($\Delta\emptyset$) of the monolayer modified ITO can be expressed as a combination of three components[53].

$$\Delta\emptyset = \Delta V_{mol} + \Delta V_{int.dip} + \Delta V_{geom.rel} \quad (1)$$

ΔV_{mol} is the component of the intrinsic dipole moment of the molecule perpendicular to the substrate surface, which induces an electrostatic potential energy change across the adsorbed monolayer. $\Delta V_{int.dip}$ is the contribution of the dipole formed at the very interface between the molecular layer and surface due to charge redistribution resulting from the interaction with the substrate. $\Delta V_{geom.rel}$ is the WF change of the bare surface due to the geometric relaxations, which is often regarded as a minor contributor. In our case, we also consider that the $\Delta V_{geom.rel}$ is not a significant factor due to the negligible surface geometry changes of ITO modified with the phosphonic acid based monolayer[53]. In general, the magnitudes of both $\Delta V_{int.dip}$ and ΔV_{mol} are expected to be coverage dependent owing to the

enhanced depolarization effects within densely packed dipole layers[65].

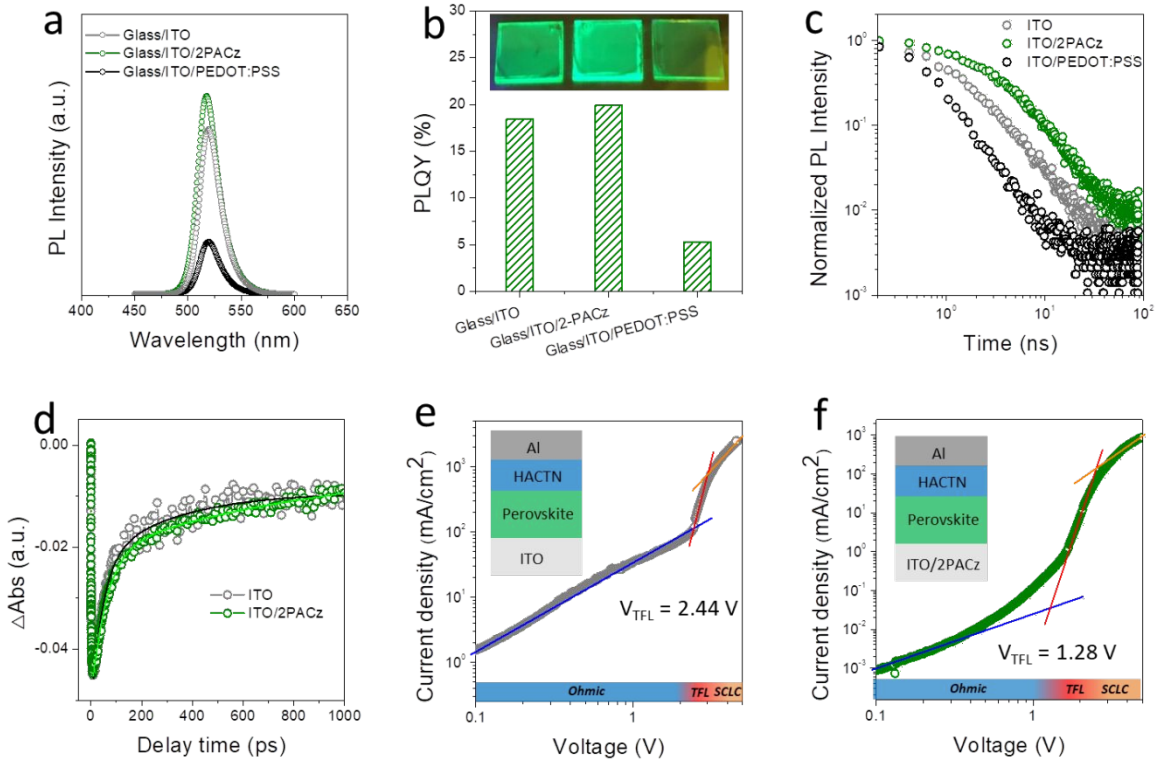

Figure 5 Effect of the HIML on the perovskite emission layer. **a-c** PL spectra **(a),** PLQYs **(b),** and time-resolved PL decay curves **(c)** of the perovskite film on the ITO, ITO/2PACz, and ITO/PEDOT:PSS substrates. **d** TA kinetics of the perovskite film on the ITO and ITO/2PACz substrates. **e-f** Dark current density-voltage curves of the hole-only device without **(e)** and with **(f)** 2PACz as HIML.

According to our UPS results of the evaporated samples, WF of bare ITO is 4.7 eV. With the gradual increase of the 2PACz thickness from 0 nm to 1 nm, the WFs increase rapidly. Then with further deposition of 2PACz, WF increase slowly, indicating that the monolayer has been formed at the thickness scale of ~1 nm[66]. Compared to the bare ITO, the WF of ITO with 2PACz monolayer (~1 nm) increases 0.32 eV (to 4.98 eV), which is almost the same as the spin-coating case (0.34 eV, shown in Fig. 4a and 4c). In fact, the growth mechanism of 2PACz on ITO based on the evaporation deposition process might be different from that in solution process, and result in more disordered packing of molecules[66]. It possibly affects the chemical bonding and degree of order of 2PACz on ITO that may correspond to the different charge transfer and the contribution of $\Delta V_{int.dip}$. From this viewpoint, we consider that in the ITO/2PACz system, ΔV_{mol} is more likely the main contributor to the WF change, rather than $\Delta V_{int.dip}$ (Fig. 4d), which agrees well with the previous theoretical and experimental findings of ITO/phosphonic acid systems[53, 67, 68]. Furthermore, we also compared the device performance of the green emission PeLEDs with solution based (using 1 mg/mL 2PACz/ethanol solution) and evaporation based (~1 nm) 2PACz HIML on ITO. As shown in Fig. S10, both of them show similar EL performance, including J-V-L curve and turn-on voltage. These results further corroborate our proposal that ΔV_{mol} is the main contributor to the WF change of ITO/2PACz.

For the fabrication of green emission PeLEDs, we used the typical phenylethylammonium bromide (PEABr) based quasi-2D $CsPbBr_3$ perovskite as the emission layer, of which the UPS spectra were also measured and shown in Fig. S11. We can estimate that the perovskite emission layer has a valence band maximum (VBM) of 5.43 eV. Overall, as shown in Fig. 4e, compared to the bare ITO, the relatively smaller energy offset between WF of ITO/2PACz and the VBM of perovskite (0.39 eV *vs.* 0.73 eV for solution process and 0.45 eV *vs.* 0.73 eV for evaporation method) can be identified, suggesting a significantly reduced hole injection barrier from ITO to perovskite emission layer. Hole-only devices were prepared as well to further confirm the improved hole injection with assistance of 2PACz as HIML by employing the device architecture of ITO/2PACz/perovskite/1,4,5,8,9,11-hexaazatriphenylene hexacarbonitrile (HATCN)/Al. The dark current-voltage curves are shown in Fig. 4f. The current density of the ITO/2PACz based device significantly surpasses that of the bare ITO based device, thus verifying the significant role that HIML plays in hole injection from ITO toward the perovskite film.

3.4 Effect of HIML on the perovskite emission layer

To explore the role of HIML on the growth of the perovskite emission layer, we investigated the quality of the perovskite film on ITO substrate with and without 2PACz. We first performed scanning electron microscope (SEM) measurements to study their morphology. As shown in Fig. S12, uniform polycrystalline quasi-2D perovskite films are grown on both the ITO and ITO/2PACz substrates. For these two samples, fewer

pinholes are observed for the perovskite film on the ITO/2PACz surface, which is expected to be beneficial to reduce electrical shunt paths, and could be ascribed to the good contact of the perovskite layer with the ITO surface. We then conducted X-ray diffraction (XRD) measurements to study the possible crystal structure change. As shown in Fig. S13, the diffraction peaks at around 15.1°, 21.3°, and 30.3° can be assigned to the (101), (121) and (202) planes of the orthorhombic *Pnma* $CsPbBr_3$ phase. Note that similar to the results in a previous study,[69] the (121) and (202) planes are close to the peak positions of the ITO substrate. No obvious change is observed between these two samples, which indicates the similar effects on the crystal growth of the perovskite film in the two cases of ITO/2PACz and bare ITO.

To investigate the optical property of the perovskite film on different substrates, we employed a series of optical spectroscopy techniques. Fig. S14 shows the absorption spectra of the perovskite film on ITO and ITO/2PACz, suggesting that 2PACz has almost no influence on the band gap and quantum well distribution of the quasi-2D perovskite films. However, a significant difference was observed in the PL spectra. As shown in Fig. 5a, the perovskite film on the ITO/2PACz substrate exhibits a remarkable enhancement (~20%) of PL intensity than that on the ITO substrate. The perovskite film on the ITO/PEDOT:PSS substrate was fabricated and measured as a control sample. A significant PL quenching was observed when compared to the ITO and ITO/2PACz based samples. The PL quantum efficiency (PLQY) of these three thin films were measured and shown in Fig. 5b. They follow the same trend of the PL intensity change, which are 18.42%, 19.91%, and 5.28% for ITO, ITO/2PACz, and ITO/PEDOT:PSS, respectively. To further determine the recombination kinetics of these perovskite thin films, we tracked the time-resolved PL (TRPL) decay curves under an excitation of 400 nm (Fig. 5c). The TRPL curve can be fitted with a bi-exponential function. The fast decay channel is related to the non-radiative recombination at grain boundaries and interfaces (including charge transfer and trap-assisted quenching), while the longer channel is ascribed to the radiative recombination of the perovskite film[17, 70]. The average PL lifetime can be estimated based on the following formula:

$$\tau_{ave} = \frac{A_1\tau_1^2 + A_2\tau_2^2}{A_1\tau_1 + A_2\tau_2} \quad (2)$$

All of these fitted lifetime results are summarized in Table S3. In comparison, the fraction of fast decay channel (A_1) of the perovskite film on ITO/2PACz is much smaller than other samples, indicating reduced non-radiative recombination. Owing to the better matching of energy levels between ITO and the perovskite VBM, the charge transfer between them should be more favorable. Therefore, the reduced non-radiative recombination should be largely attributed to the reduction of trap states at ITO/perovskite interface, instead of the suppression of charge transfer. The average PL lifetime for the ITO, ITO/2PACz, and ITO/PEDOT:PSS based samples are 3.31, 5.66, 0.72 ns, respectively. The ITO/2PACz based sample exhibits the longer lifetime, suggesting that 2PACz deposited on ITO is able to reduce the trap states, thus suppress the non-radiative recombination and luminescence quenching. In addition, we also measured the TA spectra and kinetics for the perovskite film on ITO and ITO/2PACz to further identify their recombination dynamics. As shown in Fig. S15, both samples exhibit a bleach peak around ~510 nm that belongs to the 3D phase of the quasi-2D perovskite[71]. We tracked the change of ΔA (bleach recovery) at this bleach peak as a function of delay time (Fig. 5d). Both two samples can be fitted with a bi-exponential function (the fitted results are shown in Table S4). Accordingly, a slow and a fast decay kinetic, corresponding to long- and short-time constants, is τ_1 and τ_2, respectively. The fast bleach recovery kinetics are related to the trapping process by defects at the ITO or perovskite surface, while the slow kinetics (corresponding to long time scales) are dominated by exciton recombination.[41, 72] But the perovskite film on ITO/2PACz has a relatively longer exciton lifetime of 812.26 ps than the ITO based sample (250.65 ps). The much slower bleach recovery dynamic of the ITO/2PACz based perovskite sample further support the beneficial effect of 2PACz for suppression of the non-radiative recombination process at the ITO/perovskite interface.

Furthermore, based on the ITO and ITO/2PACz based hole-only devices, we also measured their trap-filling limit voltages (V_{TFL}, the kickpoint between the Ohmic region and trap-filling limit region). The trap density (N_{trap}) of these perovskite samples can be estimated based on the following equation[73, 74]:

$$N_{trap} = \frac{2V_{TFL}\varepsilon\varepsilon_0}{eL^2} \quad (3)$$

Where ε is the relative dielectric constant (~22 for the $CsPbBr_3$) [75], ε_0 is the vacuum permittivity (8.85×10^{-12} C/V•m), e is the electron charge (1.6×10^{-19} C), and L is the thickness of the perovskite film (~35 nm). As shown in Fig. 5e-f, in comparison with the ITO based device, V_{TFL} of the ITO/2PACz based device is much lower (1.28 V *vs.* 2.44 V). The trap density of the perovskite film on ITO/2PACz is calculated to be 2.54×10^{18} cm^{-3}, which is much lower than the perovskite film on ITO (4.85×10^{18} cm^{-3}). These results are almost consistent with the PL lifetime and TA kinetic results, thus greatly highlighting the significant role of the 2PACz on suppressing non-radiative recombination and luminescence quenching of the perovskite film.

3.5 Universality of the HIML based PeLEDs

Finally, blue perovskite thin films and HIML based blue PeLEDs were fabricated to demonstrate the universality of the HIML based strategy. To prepare blue emitting perovskite films (including a pure blue and sky blue one), we mixed Cl with Br in the perovskite precursor. We first measured their absorption and PL spectra. As shown in Fig. S16, with and without 2PACz on ITO, both the pure blue and sky blue perovskite samples have similar absorption features. But remarkably increased PL intensity was observed on ITO/2PACz substrate compared to the ITO substrate, indicating greatly improved radiative recombination. To further confirm this point, the perovskite thin film samples were characterized with TRPL (Fig. S17 and Table S3). The average PL lifetimes of pure blue and sky blue perovskite films on ITO/2PACz substrates are 3.23 ns and 2.99 ns, respectively, which are longer than on the pristine ITO

substrate (2.64 ns and 2.61 ns, respectively). These results clearly demonstrate the critical role of 2PACz on ITO for

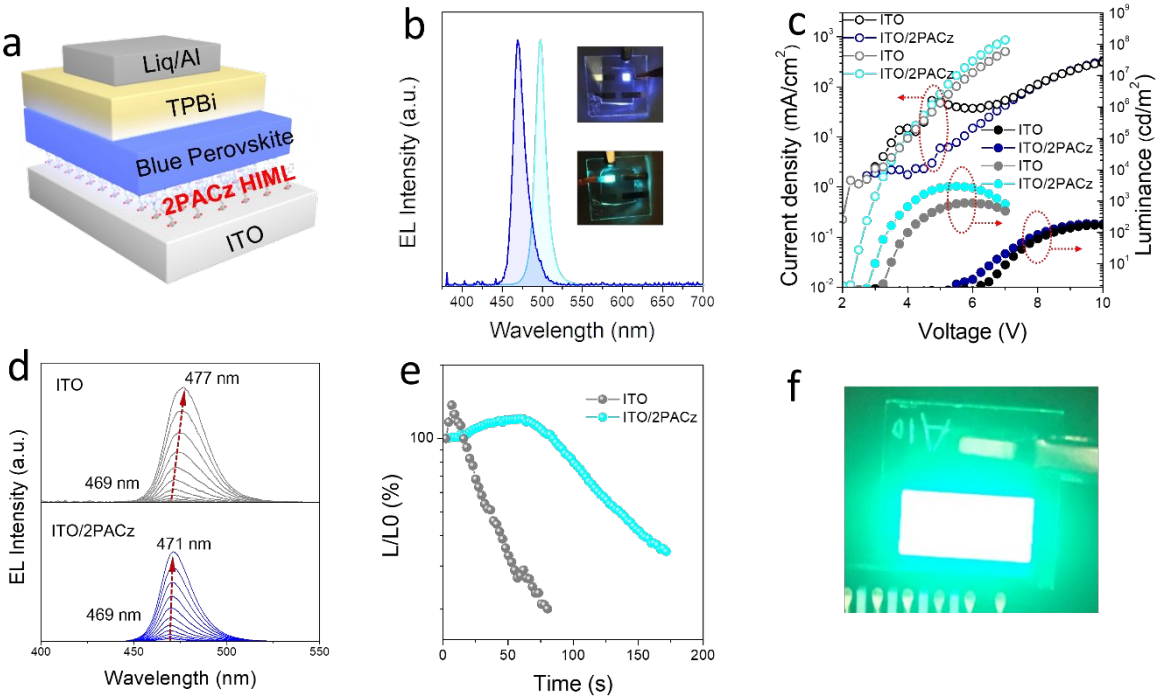

Figure 6 Universality of the HIML based PeLEDs. **a** device structure of the HIML based blue-emitting PeLEDs. **b** EL spectra of the pure-blue and sky-blue emitting PeLEDs (insets show the photographs of the working devices). **c** Current density and luminance versus driving voltage curves of the pure-blue and sky-blue emitting PeLEDs. **d** The tracked EL spectra of the pure-blue PeLEDs operated at voltages ranging from 6 to 9 V. **e** Normalized luminance-time curves operated under constant current at the initial luminance of ~100 cd/m^2 of the sky-blue PeLEDs with and without 2PACz HIML. **f** The photograph of the large-area HIML based PeLED.

interface engineering of blue emitting perovskite with suppressed non-radiative recombination.

Using the same device structure, we fabricated the pure blue and sky blue PeLEDs (Fig. 6a). The EL spectra are plotted in Fig. 6b, which show the emission wavelengths at 469 and 498 nm, with narrow FWHM (16.9 nm and 14.7 nm), respectively. The corresponding CIE color coordinates of these colorful PeLEDs are shown in Fig. S18 as well. We measured the device performance of these blue PeLEDs with and without HIML. As shown in the Fig. 6c and Fig. S19, in contrast to the bare ITO, the ITO/2PACz based pure-blue and sky-blue devices show much lower leakage current, smaller turn-on voltage, higher current density after turn-on and higher maximum luminance. Consequently, the ITO/2PACz based pure-blue and sky-blue devices exhibit higher peak EQE of 0.11% (*vs.* 0.09%) and 3.69% (*vs.* 0.85%), respectively. The possible reasons for the limited performance of blue emitting devices are inferior hole injection and low PLQYs of perovskite layers. Due to the deep VBM energy levels of the blue emitting perovskite, blue PeLEDs suffer from a large hole injection barrier between the ITO electrode (even with 2PACz HIML modification) and the perovskite emission layer, resulting in the imbalanced injection of charge carriers. Additionally, to increase the bandgap of the perovskite film, especially for the pure-blue PeLED device, some Cl anions were introduced into the perovskite film. The high concentration of Cl anions in the perovskite film can lead to deep trap states and give rise to relatively low PLQY and poor device performance.[76] But these performance results follow the similar trend as observed in the case of green emitting PeLEDs, which further demonstrates the critical role of HIML in facilitating hole injection and interfacial modification effect. More importantly, the spectra stability issue is a critical challenge for mixed halide perovskite emitters, especially for the pure blue with higher Cl content[51]. We tracked EL spectra of the pure blue PeLEDs. As shown in Fig. 6d and Fig. S20 the EL spectra of the bare ITO based pure blue device exhibited a gradual red-shifted (~8 nm) from 469 nm to 477 nm within 6-9 V range. By contrast, the EL spectra of ITO/2PACz based pure blue device seems to be much stable without obvious EL shift (only ~2 nm). For the sky blue PeLEDs, their operational stability was measured at the initial luminance of 100 cd/m^2. As shown in Fig. 6e, similar to the green emitting devices, the ITO/2PACz based sky blue PeLED has a much longer T_{50} (~135 s) than the bare ITO based device (the T_{50} is only ~37 s).

Considering the simple and cost effective fabrication process of HIML, the HIL strategy possesses great potential for large area PeLEDs, which is promising for their practical applications in solid-state display and lighting in the future. Herein, with the assistance of HIML on ITO, we fabricated a large area green emitting PeLED with device area of ~60 mm^2. Fig. 6f presents a photograph of the representative large-area HIML based PeLED. After turning on, it shows bright and uniform green emission from the device area with a maximum luminance of 4656 cd/m^2 and a peak EQE of 3.1% (Fig. S21).

4. Conclusions

In summary, we have demonstrated a general strategy of the HIML for low cost efficient PeLEDs toward reducing performance-cost gap. Through the systematic study of the interface engineering between ITO and perovskite with 2PACz as a HIML, we are able to gain a comprehensive insight into the effect of 2PACz on the device performance. In particular, with the thickness dependent UPS study, we figure out the work function change mechanism that mainly originated from the molecular dipole contribution of 2PACz. Overall, the employment of 2PACz based HIML was found to be beneficial for hole injection from ITO to perovskite, and also in favor of reducing non-radiative recombination and suppressing luminescence quenching at the ITO/perovskite interface. Finally, we verified the good universality of our HIML based strategy by demonstrating efficient blue PeLEDs and large area devices. Given the rich diversity of the HIML chemistry, we foresee usage of more versatile HIML candidates with improved capabilities for PeLEDs in the future.

Conflicts of interest

There are no conflicts to declare.

Author contributions

Y.B.Q. supervised the project. C.Z. and S.M. conceived the idea. C.Z. designed the experiments, prepared the perovskite light emitting diodes and performed the characterizations, except for those measurements mentioned below. S.M. helped fabricate SAM. L.K.O. and P.J. provided support for the analysis of XPS/UPS data and the SAM thickness estimation. C.D. helped perform the contact angle measurements. K.L. and R.K. helped perform the TA spectroscopy measurements and data analysis. Caiyi Zhang provided support for the SEM measurements. S.Y., J.Z. and T.W. provided valuable suggestions. All authors contributed to writing the paper.

Acknowledgements

This work was supported by funding from the Energy Materials and Surface Sciences Unit of the Okinawa Institute of Science and Technology Graduate University, the OIST R&D Cluster Research Program, the OIST Proof of Concept (POC) Program, and JST A-STEP Grant Number JPMJTM20HS, Japan. We thank the OIST Micro/Nanofabrication Section and Imaging Section for the support.

Notes and references

1. X.-K. Liu, W. Xu, S. Bai, Y. Jin, J. Wang, R. H. Friend and F. Gao, *Nat. Mater.*, 2020, **20**, 10-21.
2. S. Stranks and H. Snaith, *Nat. Nanotechnol.*, 2015, **10**, 391-402.
3. C. Y. Zhang, B. Wang, W. B. Li, S. Q. Huang, L. Kong, Z. C. Li and L. Li, *Nat. Commun.*, 2017, **8**, 1-9.
4. Z.-K. Tan, R. S. Moghaddam, M. L. Lai, P. Docampo, R. Higler, F. Deschler, M. Price, A. Sadhanala, L. M. Pazos, D. Credgington and F. Hanusch, *Nat. Nanotechnol.*, 2014, **9**, 687-692.
5. H. Cho, J. S. Kim, C. Wolf, Y.-H. Kim, H. J. Yun, S.-H. Jeong, A. Sadhanala, V. Venugopalan, J. W. Choi and C.-L. Lee, *ACS Nano*, 2018, **12**, 2883-2892.
6. M. Yuan, L. N. Quan, R. Comin, G. Walters, R. Sabatini, O. Voznyy, S. Hoogland, Y. Zhao, E. M. Beauregard and P. Kanjanaboos, *Nat. Nanotechnol.*, 2016, **11**, 872.
7. N. Wang, L. Cheng, R. Ge, S. Zhang, Y. Miao, W. Zou, C. Yi, Y. Sun, Y. Cao, R. Yang and Y. Wei, *Nat. Photonics*, 2016, **10**, 699.
8. D. Ma, K. Lin, Y. Dong, H. Choubisa, A. H. Proppe, D. Wu, Y.-K. Wang, B. Chen, P. Li and J. Z. Fan, *Nature*, 2021, **599**, 594-598.
9. C. Qin, T. Matsushima, W. J. Potscavage, A. S. Sandanayaka, M. R. Leyden, F. Bencheikh, K. Goushi, F. Mathevet, B. Heinrich, G. Yumoto and Y. Kanemitsu, *Nat. Photonics*, 2020, **14**, 70-75.
10. Y. Shang, G. Li, W. Liu and Z. J. A. F. M. Ning, *Adv. Funct. Mater.*, 2018, **28**, 1801193.
11. K. Lin, J. Xing, L. N. Quan, F. P. G. de Arquer, X. Gong, J. Lu, L. Xie, W. Zhao, D. Zhang and C. Yan, *Nature*, 2018, **562**, 245.
12. M. Liu, Q. Wan, H. Wang, F. Carulli, X. Sun, W. Zheng, L. Kong, Q. Zhang, C. Zhang and Q. Zhang, *Nat. Photonics*, 2021, **15**, 379-385.
13. Y. Liu, J. Y. Cui, K. Du, H. Tian, Z. F. He, Q. H. Zhou, Z. L. Yang, Y. Z. Deng, D. Chen, X. B. Zuo, Y. Ren, L. Wang, H. M. Zhu, B. D. Zhao, D. W. Di, J. P. Wang, R. H. Friend and Y. Z. Jin, *Nat. Photonics*, 2019, **13**, 760-764.
14. Z. Xiao, R. Kerner, L. Zhao, N. Tran and K. Lee, *Nat. Photonics*, 2017, **11**, 108-115.
15. B. Zhao, S. Bai, V. Kim, R. Lamboll, R. Shivanna, F. Auras, J. M. Richter, L. Yang, L. Dai and M. Alsari, *Nat. Photonics*, 2018, **12**, 783-789.
16. Y. Cao, N. Wang, H. Tian, J. Guo, Y. Wei, H. Chen, Y. Miao, W. Zou, K. Pan, Y. He and H. Cao, *Nature*, 2018, **562**, 249.
17. H. Cho, S.-H. Jeong, M.-H. Park, Y.-H. Kim, C. Wolf, C.-L. Lee, J. H. Heo, A. Sadhanala, N. Myoung, S. Yoo and S. H. Im, *Science*, 2015, **350**, 1222-1225.
18. W. D. Xu, Q. Hu, S. Bai, C. X. Bao, Y. F. Miao, Z. C. Yuan, T. Borzda, A. J. Barker, E. Tyukalova, Z. J. Hu, M. Kawecki, H. Y. Wang, Z. B. Yan, X. J. Liu, X. B. Shi, K. Uvdal, M. Fahlman, W. J. Zhang, M. Duchamp, J. M. Liu, A. Petrozza, J. P. Wang, L. M. Liu, W. Huang and F. Gao, *Nat. Photonics*, 2019, **13**, 418-424.
19. H. Wang, X. Zhang, Q. Wu, F. Cao, D. Yang, Y. Shang, Z. Ning, W. Zhang, W. Zheng and Y. Yan, *Nat. Commun.*, 2019, **10**, 1-10.
20. Y.-H. Kim, S. Kim, A. Kakekhani, J. Park, J. Park, Y.-H. Lee, H. Xu, S. Nagane, R. B. Wexler and D.-H. Kim, *Nat. Photonics*, 2021, **15**, 148-155.
21. Y. Dong, Y.-K. Wang, F. Yuan, A. Johnston, Y. Liu, D. Ma, M.-J. Choi, B. Chen, M. Chekini, S.-W. Baek and L. K. Sagar, *Nat. Nanotechnol.*, 2020, **15**, 668-674.
22. T. Chiba, Y. Hayashi, H. Ebe, K. Hoshi, J. Sato, S. Sato, Y.-J. Pu, S. Ohisa and J. Kido, *Nat. Photonics*, 2018, **12**, 681-687.
23. Z. Liu, W. Qiu, X. Peng, G. Sun, X. Liu, D. Liu, Z. Li, F. He, C. Shen and Q. Gu, *Adv. Mater.*, 2021, **33**, 2103268.
24. Z. Chu, Q. Ye, Y. Zhao, F. Ma, Z. Yin, X. Zhang and J. You, *Adv. Mater.*, 2021, **33**, 2007169.
25. Y.-H. Kim, J. Park, S. Kim, J. S. Kim, H. Xu, S.-H. Jeong, B. Hu and T.-W. Lee, *Nat. Nanotechnol.*, 2022, DOI: 10.1038/s41565-022-01113-4, 1-8.
26. B. Zhao, Y. Lian, L. Cui, G. Divitini, G. Kusch, E. Ruggeri, F. Auras, W. Li, D. Yang and B. Zhu, *Nature Electronics*, 2020, **3**, 704-710.
27. C. Jang, A. Harit, S. Lee, S. Kim and J.-E. Jeong, *ACS Nano*, 2020, **14**, 13246-13255.

28. Q. Zhang, Y.-H. Song, J.-M. Hao, Y.-F. Lan, L.-Z. Feng, X.-C. Ru, J.-J. Wang, K.-H. Song, J.-N. Yang and T. Chen, *J. Am. Chem. Soc.*, 2022, **144**, 8162-8170.
29. Y. Shen, K.-C. Shen, Y.-Q. Li, M. Guo and J. Wang, *Adv. Funct. Mater.*, 2021, **31**, 2006736.
30. Y. K. Chih, J. C. Wang, R. T. Yang, C. C. Liu, Y. C. Chang, Y. S. Fu, W. C. Lai, P. Chen, T. C. Wen, Y. C. Huang and C.-S. Tsao, *Adv. Mater.*, 2016, **28**, 8687-8694.
31. S. Lee, D. B. Kim, I. Hamilton, M. Daboczi, Y. S. Nam, B. R. Lee, B. Zhao, C. H. Jang, R. H. Friend and J. S. Kim, *Adv. Sci.*, 2018, **5**, 1801350.
32. A. Ulman, *Chem. Rev.*, 1996, **96**, 1533-1554.
33. E. Aktas, N. Phung, H. Köbler, D. A. González, M. Méndez, I. Kafedjiska, S.-H. Turren-Cruz, R. Wenisch, I. Lauermann and A. Abate, *Energy Environ. Sci.*, 2021, **14**, 3976-3985.
34. B. de Boer, A. Hadipour, M. M. Mandoc, T. van Woudenbergh and P. W. Blom, *Adv. Mater.*, 2005, **17**, 621-625.
35. G.-H. Kim, F. P. García de Arquer, Y. J. Yoon, X. Lan, M. Liu, O. Voznyy, Z. Yang, F. Fan, A. H. Ip and P. Kanjanaboos, *Nano Lett.*, 2015, **15**, 7691-7696.
36. H. Yan, Q. Huang, J. Cui, J. G. Veinot, M. M. Kern and T. J. Marks, *Adv. Mater.*, 2003, **15**, 835-838.
37. B. Choi, J. Rhee and H. H. Lee, *Appl. Phys. Lett.*, 2001, **79**, 2109-2111.
38. F. Huang, H. Liu, X. Li and S. Wang, *Nano Energy*, 2020, **78**, 105399.
39. S. Kobayashi, T. Nishikawa, T. Takenobu, S. Mori, T. Shimoda, T. Mitani, H. Shimotani, N. Yoshimoto, S. Ogawa and Y. Iwasa, *Nat. Mater.*, 2004, **3**, 317-322.
40. J. H. Schön, H. Meng and Z. Bao, *Nature*, 2001, **413**, 713-716.
41. A. Magomedov, A. Al-Ashouri, E. Kasparavičius, S. Strazdaite, G. Niaura, M. Jošt, T. Malinauskas, S. Albrecht and V. Getautis, *Adv. Energy Mater.*, 2018, **8**, 1801892.
42. E. Yalcin, M. Can, C. Rodriguez-Seco, E. Aktas, R. Pudi, W. Cambarau, S. Demic and E. Palomares, *Energy Environ. Sci.*, 2019, **12**, 230-237.
43. A. Ullah, K. H. Park, H. D. Nguyen, Y. Siddique, S. Shah, H. Tran, S. Park, S. I. Lee, K. K. Lee and C. H. Han, *Adv. Energy Mater.*, 2022, **12**, 2103175.
44. A. Al-Ashouri, E. Köhnen, B. Li, A. Magomedov, H. Hempel, P. Caprioglio, J. A. Márquez, A. B. Morales Vilches, E. Kasparavicius and J. A. Smith, *Science*, 2020, **370**, 1300-1309.
45. G. Kapil, T. Bessho, Y. Sanehira, S. R. Sahamir, M. Chen, A. K. Baranwal, D. Liu, Y. Sono, D. Hirotani and D. Nomura, *ACS Energy Lett.*, 2022, **7**, 966-974.
46. A. Al-Ashouri, A. Magomedov, M. Roß, M. Jošt, M. Talaikis, G. Chistiakova, T. Bertram, J. A. Márquez, E. Köhnen and E. Kasparavičius, *Energy Environ. Sci.*, 2019, **12**, 3356-3369.
47. X. Deng, F. Qi, F. Li, S. Wu, F. R. Lin, Z. Zhang, Z. Guan, Z. Yang, C.-S. Lee and A. K.-Y. Jen, *Angew. Chem. Int. Ed.*, 2022, DOI: 10.1002/anie.202203088, doi.org/10.1002/anie.202203088.
48. M. Roß, S. Severin, M. B. Stutz, P. Wagner, H. Köbler, M. Favin-Lévêque, A. Al-Ashouri, P. Korb, P. Tockhorn and A. Abate, *Adv. Energy Mater.*, 2021, **11**, 2101460.
49. M. Gedda, D. Gkeka, M. I. Nugraha, A. D. Scaccabarozzi, E. Yengel, J. I. Khan, I. Hamilton, Y. Lin, M. Deconinck and Y. Vaynzof, *Adv. Energy Mater.*, 2022, DOI: 10.1002/aenm.202201396, 2201396.
50. Y. S. Shin, S. Ameen, E. Oleiki, J. Yeop, Y. Lee, S. Javaid, C. B. Park, T. Song, D. Yuk and H. Jang, *Adv. Opt. Mater.*, 2022, DOI: 10.1002/adom.202201313, 2201313.
51. Y. Liu, L. K. Ono, G. Tong, T. Bu, H. Zhang, C. Ding, W. Zhang and Y. B. Qi, *J. Am. Chem. Soc.*, 2021, **143**, 19711-19718.
52. Y. Liu, L. K. Ono, G. Tong, H. Zhang and Y. Qi, *ACS Energy Lett.*, 2021, **6**, 908-914.
53. S. A. Paniagua, A. J. Giordano, O. N. L. Smith, S. Barlow, H. Li, N. R. Armstrong, J. E. Pemberton, J.-L. Bredas, D. Ginger and S. R. Marder, *Chem. Rev.*, 2016, **116**, 7117-7158.
54. Y. Lin, Y. Firdaus, F. H. Isikgor, M. I. Nugraha, E. Yengel, G. T. Harrison, R. Hallani, A. El-Labban, H. Faber and C. Ma, *ACS Energy Lett.*, 2020, **5**, 2935-2944.
55. H. Kim, J. S. Kim, J.-M. Heo, M. Pei, I.-H. Park, Z. Liu, H. J. Yun, M.-H. Park, S.-H. Jeong and Y.-H. J. N. c. Kim, *Nat. Commun.*, 2020, **11**, 1-13.
56. F. Ye, Q. Shan, H. Zeng and W. C. Choy, *ACS Energy Lett.*, 2021, **6**, 3114-3131.
57. T. R. Gengenbach, G. H. Major, M. R. Linford, C. D. J. J. o. V. S. Easton, S. Technology A: Vacuum and Films, *Journal of Vacuum Science & Technology A*, 2021, **39**, 013204.
58. P. Prieto, V. Nistor, K. Nouneh, M. Oyama, M. Abd-Lefdil and R. J. A. S. S. Díaz, *Appl. Surf. Sci.*, 2012, **258**, 8807-8813.
59. J. H. Seo, R. Yang, J. Z. Brzezinski, B. Walker, G. C. Bazan and T. Q. Nguyen, *Adv. Mater.*, 2009, **21**, 1006-1011.
60. N. Dam, M. Beerbom, J. Braunagel and R. Schlaf, *J. Appl. Phys.*, 2005, **97**, 024909.
61. A. Laforgue, T. Addou and D. Bélanger, *Langmuir*, 2005, **21**, 6855-6865.
62. M. Textor, L. Ruiz, R. Hofer, A. Rossi, K. Feldman, G. Hähner and N. D. Spencer, *Langmuir*, 2000, **16**, 3257-3271.
63. C. L. Perkins, *J. Phys. Chem. C*, 2009, **113**, 18276-18286.
64. W. Yang, A. Broski, J. Wu, Q. H. Fan and W. Li, *IEEE Trans. Nanotechnol.*, 2017, **17**, 701-704.
65. H. K. Kim, A. S. Hyla, P. Winget, H. Li, C. M. Wyss, A. J. Jordan, F. A. Larrain, J. P. Sadighi, C. Fuentes-Hernandez and B. Kippelen, *Chem. Mater.*, 2017, **29**, 3403-3411.
66. F. Widdascheck, A. A. Hauke and G. Witte, *Adv. Funct. Mater.*, 2019, **29**, 1808385.
67. P. J. Hotchkiss, H. Li, P. B. Paramonov, S. A. Paniagua, S. C. Jones, N. R. Armstrong, J. L. Brédas and S. R. Marder, *Adv. Mater.*, 2009, **21**, 4496-4501.
68. H. Li, P. Paramonov and J.-L. Bredas, *J. Mater. Chem.*, 2010, **20**, 2630-2637.
69. J. H. Warby, B. Wenger, A. J. Ramadan, R. D. Oliver, H. C. Sansom, A. R. Marshall and H. J. Snaith, *ACS Nano*, 2020, **14**, 8855-8865.
70. B. R. Lee, J. C. Yu, J. H. Park, S. Lee, C.-K. Mai, B. Zhao, M. S. Wong, E. D. Jung, Y. S. Nam and S. Y. Park, *ACS Nano*, 2018, **12**, 5826-5833.
71. L. N. Quan, Y. Zhao, F. P. García de Arquer, R. Sabatini, G. Walters, O. Voznyy, R. Comin, Y. Li, J. Z. Fan and H. Tan, *Nano Lett.*, 2017, **17**, 3701-3709.
72. M. C. Gélvez-Rueda, M. B. Fridriksson, R. K. Dubey, W. F. Jager, W. Van der Stam and F. C. J. N. c. Grozema, *Nat. Commun.*, 2020, **11**, 1-9.
73. E. A. Duijnstee, J. M. Ball, V. M. Le Corre, L. J. A. Koster, H. J. Snaith and J. Lim, *ACS Energy Lett.*, 2020, **5**, 376-384.
74. J. Chen and N. G. Park, *Adv. Mater.*, 2019, **31**, 1803019.
75. M. I. Saidaminov, M. A. Haque, J. Almutlaq, S. Sarmah, X. H. Miao, R. Begum, A. A. Zhumekenov, I. Dursun, N. Cho and B. Murali, *Adv. Opt. Mater.*, 2017, **5**, 1600704.
76. Y.-H. Zhou, C. Wang, S. Yuan, C. Zou, Z. Su, K.-l. Wang, Y. Xia, B. Wang, D. Di and Z.-K. J. J. o. t. A. C. S. Wang, *J. Am. Chem. Soc.*, 2022, **144**, 18470-18478.